IEEE Access
Multidisciplinary ⋮ Rapid Review ⋮ Open Access Journal

Received February 28, 2017, accepted March 23, 2017, date of publication May 8, 2017, date of current version June 28, 2017.

Digital Object Identifier 10.1109/ACCESS.2017.2702205

Numerical Analysis of a Transmission Line Illuminated by a Random Plane-Wave Field Using Stochastic Reduced Order Models

ZHOUXIANG FEI, YI HUANG, (Senior Member, IEEE), JIAFENG ZHOU, AND CHAOYUN SONG, (Student Member, IEEE)

Department of Electrical Engineering and Electronics, The University of Liverpool, Liverpool L69 3GJ, U.K.

Corresponding author: Yi Huang (e-mail: yi.huang@liv.ac.uk)

This work was supported in part by the ICE-NITE Project (a Collaborative Research Project funded by the Innovate U.K.) under Contract 101665, in part by BAE Systems Ltd., in part by HORIBA MIRA, Ltd., in part by the International TechneGroup Ltd., and in part by the University of Nottingham.

ABSTRACT A novel nonintrusive statistical approach, known as the stochastic reduced order model (SROM) method, is applied to efficiently estimate the statistical information of the terminal response (i.e., the induced current) in transmission lines excited by a random incident plane-wave field. The idea of the SROM method is conceptually simple, i.e., to represent the uncertain input space dimensioned by random variables using the SROM-based input model. This input model consists of a very small number of selected samples with assigned probabilities. Thus, only these input samples in the model need to be evaluated using the deterministic solver. The SROM-based output model can be constructed to approximate the propagated uncertainty to the real output response with elementary calculation. The efficiency and accuracy of the SROM method to obtain the statistics of the induced current are analyzed using two examples, where the complexity of the uncertain input space gradually increases. The performance of the SROM method is compared with that of the traditional Monte Carlo (MC) method. The stochastic collocation (SC) method based on sparse grid sampling strategy computed via the Smolyak algorithm is also implemented to fairly evaluate the SROM performance. The result shows that the SROM method is much more efficient than the MC method to obtain accurate statistics of the induced current, and even shows a faster convergence rate compared with that of the SC method in the examples considered. Therefore, the SROM method is a suitable approach to investigate the variability of radiated susceptibility in electromagnetic compatibility problems with a random incident wave.

INDEX TERMS Field-to-wire coupling, stochastic collocation, stochastic reduced order model (SROM), transmission lines, uncertainty quantification.

I. INTRODUCTION

The induced effect in cables caused by an incident electromagnetic field may be a potential threat to degrade the performance of the system. This phenomenon is especially of interest in aerospace systems. Therefore, it is important to estimate the terminal response (such as the induced current or voltage) of the cable to the impinging electromagnetic field at the early stage to prevent possible malfunctions.

For deterministic estimation, the pioneering work in [1] gave a closed-form solution for the terminal response of a two-conductor transmission line illuminated by an incident field. This work was later generalized for multiconductor transmission lines (MTLs) in [2] and [3]. Then, the field-to-wire coupling model was extended for some common configurations, such as a twisted-wire pair (TWP) in free space [4], a TWP or a bundle of TWPs above a ground plane in [5] and [6]. The estimation approach for nonuniform cable types (i.e., the cross-section varies along the cable length) was addressed in [7] and [8]. The induced effect resulting from the strong electromagnetic field such as lightning strikes was investigated in [9] and [10].

The aforementioned work is very useful for deterministic analysis with a unique output, but may not be sufficient for practical cases. This is because the characteristics of the incident wave (such as the field strength and incident direction) could be unknown in practice. As a result, statistical analysis needs to be performed to account for the potential variability of the induced effect.

If the deterministic solver relating the input to output takes the form of an analytic formula, the theory of random variable transformation in [11] can be used to obtain the statistical information of the output. On this basis, pioneering contributions were presented in [12] and [13] to derive closed-form expressions for the statistical properties of the induced current. However, the probabilistic transformation involved may become prohibitively difficult if the deterministic solver takes complex algebraic forms or is an electromagnetic simulator. Other work was dedicated to the estimation of extreme induced current values using the controlled stratification method [14].

In order to perform a general statistical analysis, one may consider using the conventional Monte-Carlo (MC) method [15], the well-established polynomial chaos expansion (PCE) [16] and stochastic collocation (SC) [17] methods, and the newly proposed *stochastic reduced order model* (SROM) method [18]. The MC method is nonintrusive, as the deterministic solver is used without any modifications. However, the MC method may only produce converged results after examining a sufficient number of possible occurrences, and therefore, is inefficient. Applications of the MC method for field-to-wire coupling problems can be found in [19] and [20].

The PCE method [16] has been used as an efficient statistical tool in the last decade. This method can express the deterministic solver using an analytical formula with regard to uncertain input variables. This analytical formula is used as a replacement for the original deterministic solver. On this basis, the statistics of the output can be efficiently obtained. An application of the PCE method was given in [21] to estimate the statistics of the induced current at the termination load of transmission lines.

Similar to the PCE method, the SC method [17] is also aimed at expressing the deterministic solver using an analytical formula. How to perform the SC method was given in [17] and [22]. Like the MC method, the SC method is also nonintrusive.

The SROM method [18] was recently proposed as a computationally efficient alternative to MC simulations for statistical analysis. This method is general, nonintrusive, and able to produce accurate output statistics by only using a small fraction of the MC computational cost. The idea of the SROM method is essentially different from those of the PCE and SC methods, but to approximate the statistics of random input variables by using a very small number of selected samples assigned with probabilities. Therefore, unlike the MC method looking blindly and exhaustively at all the possible cases, the SROM method only needs to examine these selected samples without sacrificing accuracy. Clearly, the SROM method can be considered as a smart version of the MC method. The first application of the SROM method for EMC problems was dedicated to the statistical analysis of cable crosstalk in [23].

Since SROM is a novel methodology, it is worth another specific investigation on its performances and advantages versus the brute-force MC approach and other efficient statistical methods. In this paper, the SROM method is applied to efficiently estimate the statistics of the induced current in multiconductor transmission lines induced by a random incident wave. It provides an incremental contribution to efficient statistical analysis of field-to-wire coupling problems. Also, as the relative goodness of SROM over SC or vice versa in terms of efficiency is still unexplored, the SROM performance is also compared with the SC method based on Lagrange polynomials. The remainder of the paper is organized as follows: Section II presents a concise introduction of the SROM method. In Section III, the field-to-wire coupling model is described. In Section IV, the implementation of SROM for uncertainty propagation in the case considered is presented. Also, the application of the SC method is briefly presented for comparison purposes. The discussion about the SROM and SC performances is given in Section V. The conclusion of the paper is presented in Section VI.

II. STOCHASTIC REDUCED ORDER MODEL (SROM)

An introduction of the SROM method is presented in this section. Let $\boldsymbol{X} = [X_1, X_2, \ldots, X_D]$ be a D-dimensional random input variable. Each dimension X_i $(1 \le i \le D)$ is used to describe the variation of a random variable, and can be correlated or uncorrelated with other dimensions. The statistical properties of $\boldsymbol{X}$ are assumed to be known beforehand. According to [24], they are described by the cumulative distribution function (CDF) and q-th order moment of the i-th dimension X_i in (1) and (2), respectively, and the correlation function in (3):

$$F_i(\theta) = P(X_i \le \theta) \tag{1}$$

$$\mu_i(q) = E\left(X_i^q\right) \tag{2}$$

$$\boldsymbol{r} = E[\boldsymbol{X}\boldsymbol{X}^T] \tag{3}$$

where $i = 1, \ldots, D$. Here, $F_i(\theta)$ is the probability of X_i taking a value smaller than or equal to θ. The operator $E(\cdot)$ means calculating the expectation value.

A. DEFINITION OF SROM

A SROM $\tilde{X}$ is a sample-probability pair $\{\tilde{\boldsymbol{x}}, \boldsymbol{p}\}$ containing a very small number of samples with assigned probabilities, in order to accurately approximate the statistics of the random variable $\boldsymbol{X}$ quantified in (1)-(3). The sample set $\tilde{\boldsymbol{x}}$ contains m different samples: $\{\tilde{\boldsymbol{x}}^{(1)} \ldots, \tilde{\boldsymbol{x}}^{(m)}\}$. The sample $\tilde{\boldsymbol{x}}^{(k)}(1 \le k \le m)$ in $\tilde{\boldsymbol{x}}$ contains a set of coordinates $(\tilde{x}_1^{(k)}, \ldots, \tilde{x}_D^{(k)})$ for $\boldsymbol{X} = [X_1, X_2, \ldots, X_D]$. For example, $\tilde{x}_1^{(k)}$ is the coordinate of $\boldsymbol{X}$ in the dimension X_1. The probability set $\boldsymbol{p}$ contains the probabilities $\{p^{(1)}, \ldots, p^{(m)}\}$ of each sample in $\tilde{\boldsymbol{x}}$. The probabilities $\{p^{(1)}, \ldots, p^{(m)}\}$ need to meet the conditions: $\sum_{k=1}^{m} p^{(k)} = 1$ and $p^{(k)} > 0$.

The sample size m of $\tilde{X}$ is related to the accuracy and computational cost. A better accuracy is usually guaranteed by increasing m, but accompanied by a brutal computational burden. Thus, choosing a proper value of m is mainly dependent on the affordable computational cost. The statistical information of $\tilde{X}$ is described by the following three counterpart parameters of those of $\boldsymbol{X}$ in (1)-(3):

$$\tilde{F}_i(\theta) = P\left(\tilde{X}_i \le \theta\right) = \sum_{k=1}^{m} p^{(k)} 1(\tilde{x}_i^{(k)} \le \theta) \tag{4}$$

$$\tilde{\mu}_i(q) = E\left(\tilde{X}_i^q\right) = \sum_{k=1}^{m} p^{(k)} (\tilde{x}_i^{(k)})^q \tag{5}$$

$$\tilde{r}_{ij} = E\left[\tilde{X}_i \tilde{X}_j\right] = \sum_{k=1}^{m} p^{(k)} \tilde{x}_i^{(k)} \tilde{x}_j^{(k)} \tag{6}$$

where $1(A)$ is the indicator function and has two possible outcomes: 1 if A is true and 0 if A is false.

Since there could exist many different SROM candidates $\tilde{\boldsymbol{X}}$ for $\boldsymbol{X}$, a measure of the discrepancy between the statistics of $\boldsymbol{X}$ and $\tilde{\boldsymbol{X}}$ is needed. Thus, the accuracy of $\tilde{\boldsymbol{X}}$ can be assessed by the summation of the discrepancies between each statistical property of $\tilde{\boldsymbol{X}}$ and $\boldsymbol{X}$ (i.e., between (1) and (4), (2) and (5), (3) and (6)). The mathematical definition of the accuracy can be found in [23]. The SROM candidate giving the most accurate approximation for the statistics of $\boldsymbol{X}$ is referred to as the optimal SROM $\tilde{\boldsymbol{X}}$. Ideally, this optimal $\tilde{\boldsymbol{X}}$ should be used in the implementation of the SROM approach. However, in practice finding the optimal $\tilde{\boldsymbol{X}}$ can be too exhaustive or even impossible. This is because the optimal $\tilde{\boldsymbol{X}}$ can only be credited after examining every possible combination of legitimate $\tilde{\boldsymbol{x}}$ and $\boldsymbol{p}$.

To solve this problem, three sampling techniques (i.e., *Dependent thinning*, *Integer optimization*, and *Pattern classification*) were suggested in [18] as guidelines on choosing the sample set $\tilde{\boldsymbol{x}}$ of $\tilde{\boldsymbol{X}}$. Which technique to use can be chosen heuristically, as all three techniques have the same aim: to select m samples scattered as far from each other as possible in the uncertain space of $\boldsymbol{X}$. Taking samples in $\tilde{\boldsymbol{x}}$ as centers of tessellations, the uncertain input space of $\boldsymbol{X}$ can be divided into m Voronoi tessellations [25]. The probability is assigned to each sample in $\tilde{\boldsymbol{x}}$ as the frequency density of the grouped data in the corresponding Voronoi tessellation. Although the resultant sample-probability pair of $\tilde{\boldsymbol{X}}$ may not be strictly optimal, it generally provides a more accurate statistical approximation of $\boldsymbol{X}$, compared with other candidates obtained using random selection. The *pattern classification* technique is used in this study to obtain the sample set $\tilde{\boldsymbol{x}}$ of $\boldsymbol{X}$. The mathematical workflow of using *pattern classification* to construct $\tilde{\boldsymbol{X}}$ can be found in [23].

B. SOLUTION BY SROM

This section describes how to propagate uncertainty from the multivariate random variable $\boldsymbol{X} = (X_1, X_2, \ldots, X_D)$ to the output $\boldsymbol{Y}$ with the SROM method. Here, $\boldsymbol{X}$ can be interpreted as a collection of D random variables. After obtaining $\tilde{\boldsymbol{X}} = \{\tilde{\boldsymbol{x}}, \boldsymbol{p}\}$ as the SROM-based input, the statistics of $\boldsymbol{Y}$ can be derived in three steps as follows:

Step 1): Construct a SROM-based output $\tilde{Y} = \{\tilde{\boldsymbol{y}}, p_y\}$ for the real output $\boldsymbol{Y}$. The sample set $\tilde{\boldsymbol{y}} = \{\tilde{\boldsymbol{y}}^{(1)}, \ldots, \tilde{\boldsymbol{y}}^{(m)}\}$ can be obtained by running the deterministic solver M with the input set equal to $(\tilde{\boldsymbol{x}}^{(1)}, \ldots, \tilde{\boldsymbol{x}}^{(m)})$, sequentially:

$$M : \tilde{\boldsymbol{x}}^{(k)} \to \tilde{\boldsymbol{y}}^{(k)}, k = 1, \ldots, m. \tag{7}$$

The probabilities $\{p_y^{(1)}, \ldots, p_y^{(m)}\}$ in the probability set $\boldsymbol{p}_Y$ can be obtained using: $p_Y^{(k)} = p^{(k)}, k = 1, \ldots, m$. This is because the occurrence of $\tilde{\boldsymbol{y}}^{(k)}$ is completely subject to the occurrence of $\tilde{\boldsymbol{x}}^{(k)}$.

Step 2): The CDF, q-th order moment, and standard deviation of $\tilde{\boldsymbol{Y}}$ can be obtained using:

$$P\left(\tilde{\boldsymbol{Y}} \le \xi\right) = \sum_{k=1}^{m} p^{(k)} \boldsymbol{I}(\tilde{y}^{(k)} \le \xi) \tag{8}$$

$$E\left(\tilde{Y}^q\right) = \sum_{k=1}^{m} p^{(k)} (\tilde{y}^{(k)})^q \tag{9}$$

$$\sigma\left(\tilde{Y}\right) = \sum_{k=1}^{m} p^{(k)} \left(\tilde{y}^{(k)} - E(\tilde{Y}^1)\right)^2. \tag{10}$$

Step 3): The statistical information of the actual output $\boldsymbol{Y}$ is approximated by those of the SROM-based output $\tilde{Y}$ in (8)–(10).

The reason for the SROM method being able to reduce computational cost is now clear: only a small number of representative samples ($\tilde{\boldsymbol{x}}^{(1)}, \ldots, \tilde{\boldsymbol{x}}^{(m)}$) needs to be checked. In contrast, the MC method exhaustively examines almost every input sample until the converged result is obtained. The only overhead of the SROM method is to build the optimal model to account for uncertainty sources, and is negligible compared with the computational cost of the MC method.

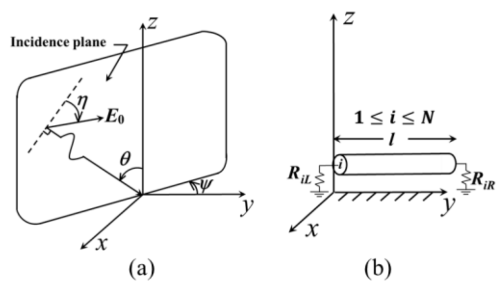

FIGURE 1. **(a) Variables characterizing the incident plane-wave field. (b) Configuration of an arbitrary wire in the illuminated MTL [26].**

III. DETERMINISTIC SYSTEM

In this section, the field-to-wire coupling model sketched in Fig. 1 is introduced. As shown in Fig. 1(a), the external excitation source is a plane-wave field characterized by the incidence angles θ (the elevation angle) and ψ (the azimuth angle), the polarization angle η, and the electric field amplitude E_0.

The victim of the incident field is a uniform and lossless MTL with length l. This MTL consists of N perfect conductors placed in the y-*axis* direction above a ground plane. For the sake of the neatness of the MTL plot, only a representative (the ith, $1 \le i \le N$) conductor is shown in Fig. 1(b).

The position of the ith conductor in the x-z plane (the cross-section plane) is denoted by the coordinate (x_i, z_i). The ith conductor is connected to the ground plane via the termination loads R_{iL} at the left end and R_{iR} at the right end. The medium immersing the MTL is characterized by the electric permittivity ε_0 and magnetic permeability μ_0 in free space. The system response refers to the induced current in the right-end termination of the MTL. Given the characteristics of the field-to-wire coupling model, the induced current can be calculated using the deterministic solver (i.e., the calculation process). The detailed description of the deterministic solver was presented in [26], and is not repeated herein.

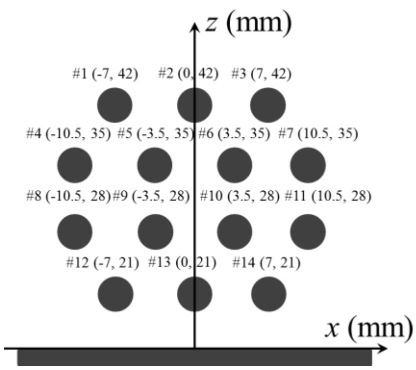

FIGURE 2. Positions of each line denoted by the coordinates (x_i, z_i) in the cross section of the MTL.

TABLE 1. Clarification of stochastic and deterministic variables.

θ	Stochastic
ψ	Stochastic
E_0	Deterministic in Section IV.A, stochastic in Section IV.B.
η	Deterministic in Section IV.A, stochastic in Section IV.B.
x_i	Deterministic
z_i	Deterministic
R_{iL}	Deterministic
R_{iR}	Deterministic

The uncertainty is assumed to be embedded in the incident field, whereas the features of the MTL are deterministically characterized. Specifically, the length of the MTL is $l = 2$ m, and the radius of each conductor is $r = 1$ mm. The cross-section detail of the MTL is shown in Fig. 2. Each line is terminated using 50 Ω loads at the left and right ends. By default, the analysis is performed at the frequency of 50 MHz unless specifically stated. A clarification of the stochastic and deterministic variables assumed in this paper is given in Table 1.

IV. NUMERICAL EXAMPLES

In this section, taking the MTL with 14 conductors as the victim, the SROM method is applied to derive the statistics of the induced current excited by a random incident plane-wave. Specifically, the induced current (I_{R3}) in the right-end termination of wire #3 is observed for the demonstration purpose.

To test the efficacy and robustness of the proposed SROM method, two examples are considered, and the complexity of the uncertain input space in the second example is increased with respect to the first one. In addition, the SC method using Lagrange interpolation is also applied to random field coupling problems for the first time. But the aim of introducing the SC method is to provide a competing technique for comparison with the SROM method. MC results from 200000 simulations are used as the reference to benchmark the accuracy of the SROM and SC results.

A. RANDOM θ AND ψ

In this section, the SROM method is applied to quantify the variability of the induced current I_{R3} due to two uncertain variables, and its performance is discussed with respect to the SC method. The two random variables are chosen as the incidence angles θ and ψ following uniform distributions in $[0, \pi/2]$ and $[0, \pi]$, respectively. This assumption means that the incident plane-wave field could illuminate the MTL from any direction above the ground plane. Please note that the variation range of the azimuth ψ is chosen as $[0, \pi]$ instead of $[0, 2\pi]$. This is because the cross section of the MTL is symmetrical. Such a choice can avoid analyzing a redundant space of the variable ψ. It is to be noted that the random variables in this paper are uncorrelated by nature, but the SROM method is also applicable to correlated input variables, please see [18] for example. The field strength E_0 and polarization angle η are assumed to take deterministic values of 1 V/m and 0∘, respectively.

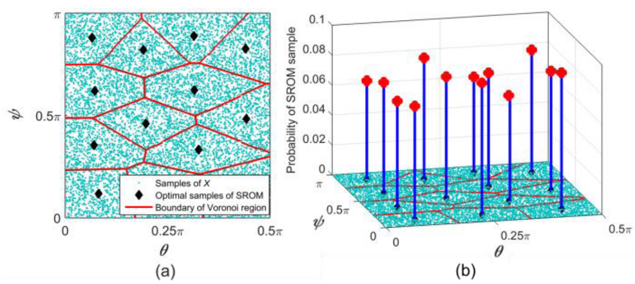

FIGURE 3. (a) Distribution of 10000 samples of $X = [\theta, \psi]$ and 13 samples of $\tilde{X}$ in corresponding Voronoi regions. (b) Visualization of SROM $\tilde{X}$ with sample size of 13.

The first step of the SROM implementation process is to construct a SROM-based input model as the approximation of the uncertain input space. Let $\boldsymbol{X}$ be a bivariate random variable containing the two uncertain variables θ and ψ, i.e., $\boldsymbol{X} = [\theta, \psi]$ and the dimension $D = 2$. Each sample of $\boldsymbol{X}$ represents a point on the 2-D plane dimensioned using θ and ψ as orthogonal axes. The coordinates of the point indicate the input information, i.e., the values of θ and ψ. This information can be used to run the deterministic solver once and obtain the corresponding output value (i.e., the induced current in this case). The construction process of the SROM-based input $\tilde{\boldsymbol{X}}$ for $\boldsymbol{X}$ is visualized in Fig. 3.

As shown in Fig. 3(a), 10000 independent samples of $\boldsymbol{X} = [\theta, \psi]$ are randomly generated according to the probability distributions of θ and ψ. The samples of $\tilde{X}$ can be selected using the pattern classification algorithm, and are shown in Fig. 3(a) for sample size $m = 13$. Having determined the samples of $\tilde{X}$, the probability of the sample in $\tilde{X}$ can be obtained using the sample number of X in that specific Voronoi region. Now the SROM-based input $\tilde{X}$ is completely constructed and visualized using red dots in Fig. 3(b). Specifically, the projection of the red dot on the θ-ψ plane tells the coordinates of the SROM sample, and the height of the red dot represents the probability assigned to this SROM sample. It is clear that the SROM samples in $\tilde{X}$ are assigned very similar probabilities, and are evenly located in the uncertain region: $[0, 0.5\pi] \times [0, \pi]$. This is due to the probabilistic nature of the input X (i.e., following uniform distributions in the dimensions of θ and ψ). Please note that a different set of 10000 MC samples in Fig. 3(a) (but still accurately characterizing the statistics of the input) would yield variations in the choice of SROM samples and probabilities. But such variations are very small and the influence on the accuracy of the result is negligible. Due to the importance of assumed input statistical distributions on the result, one could also consider the influence of assuming Gaussian distributed incidence angles of the plane wave. Such an investigation would be similar to the example of bivariate Gaussian distributions in [23].

Having constructed the SROM-based input $\tilde{X}$ for $X = [\theta, \psi]$, the SROM-based output $\tilde{I_{R3}}$ can be obtained according to Section II-B. Specifically, the samples of $\tilde{I_{R3}}$ are produced using the deterministic solver, and the probabilities of the samples in $\tilde{I_{R3}}$ are the same as those in $\tilde{X}$. On this basis, the statistics (i.e., CDF, mean value, and standard deviation) of the actual induced current I_{R3} can be derived using (8)-(10).

On the other hand, the SC method is also implemented based on sparse grid sampling computed via the Smolyak algorithm. This sampling technique can significantly reduce the number of times of running the deterministic solver for high random dimensions, compared with the tensor product sampling. The SC implementation process is decomposed as follows. First, collocation points are selected in the uncertain input region using sparse grid sampling. Here, SC collocation points are essentially the same as SROM samples, in the sense that the coordinates of each collocation point also contain the value of each random variable to run the deterministic solver once. In other words, the number of collocation points is equal to the number of simulations for SC to derive the analytical relationship between random inputs and the output. The number of collocation points is determined by the random dimension D and the Smolyak construction level k. If D is fixed, the number of collocation points is increased by increasing k, so are the accuracy and computational cost. The coordinates of the collocation point in each dimension can be calculated based on the extrema of Chebyshev polynomials [17]. Having obtained collocation points, the output values at collocation points are calculated using the deterministic solver. On this basis, the Lagrange interpolating function (a common choice of polynomials in the SC implementation) can be used to derive the analytical formula representing the deterministic solver. Now the statistics (mean, standard deviation, and CDF) of the output can be extracted from the output samples obtained by evaluating a sufficient number of input samples using this analytical formula (i.e., the derived efficient form of the deterministic solver).

It is clear that the accuracy of the SC result is dependent on the resolution of the derived analytical formula with respect to the deterministic solver. Since the SC method is not the core of this study, only a concise description of the SC method is given above, and further details can be found in [17] and [22]. The SC application in this paper is realized using the sparse grid interpolation toolbox in [27].

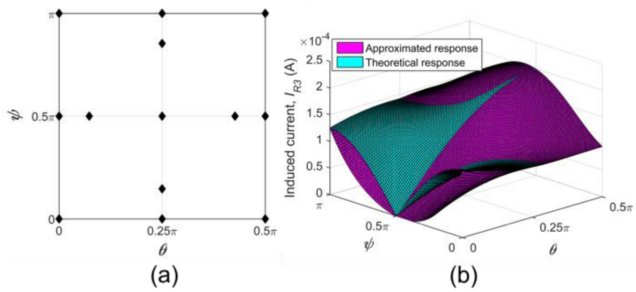

FIGURE 4. (a) 13 collocation points obtained using sparse grids based on the extrema of Chebyshev polynomials, with $D = 2$ and $k = 2$. (b) Comparison of the theoretical response and the SC approximated response using 13 collocation points.

In each comparison, the number of SROM samples is chosen the same as that of the SC collocation points. As a result, the two methods consume the same computational cost of running the deterministic solver. Fig. 4(a) shows 13 collocation points in the uncertain input region: $[0, 0.5\pi] \times [0, \pi]$, with $k = 2$. In Fig. 4(b), the derived analytical response of the induced current I_{R3} to incidence angles θ and ψ is plotted against the theoretical response (obtained from the 200000 MC simulations). In this case, the approximated response by the SC method gives exact induced currents at collocation points, but is generally very different from the theoretical response. With the approximated response of I_{R3} being obtained, the statistics of I_{R3} can be efficiently obtained. Please note that the theoretical response of this bivariate example in Fig. 4(b) does not present symmetry in the space of random variables. This implies that the proposed example is suitable for evaluation purposes, as symmetry could make SROM, SC, and MC uselessly inefficient.

In Fig. 5, the derived CDFs of I_{R3} obtained by the SROM and SC methods are compared. Here, the SROM sample number is set to 13, 29, 65, and 145, to equalize the number of SC collocation points at $k = 2$, 3, 4, and 5, respectively. Hereinafter, the sample size can refer to the SROM sample number as well as the SC collocation point number, depending on which method is being discussed. It is clear in Fig. 5 that for each method, the derived CDF becomes closer to the reference CDF (given by 200000 MC simulations) by increasing the sample size. But the performances of SROM and SC could be different. Specifically, at the sample size of 13, the

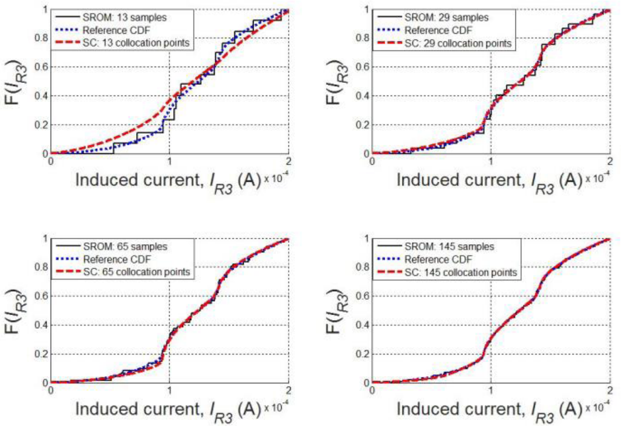

FIGURE 5. Comparison of the reference CDF of I_{R3}, the CDFs approximated by the SROM-based output $\tilde{I}_{R3}$ with the sample sizes of 13, 29, 65, and 145, and the CDFs approximated by the SC method with 13, 29, 65, and 145 collocation points (corresponding to $k = 2$, 3, 4, and 5, respectively).

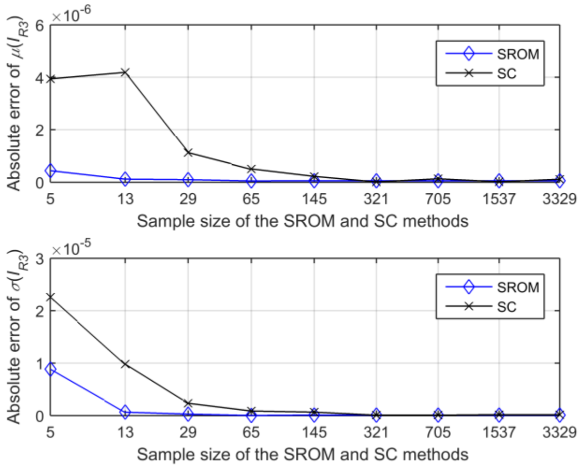

FIGURE 6. Convergence rates of the SROM and SC methods at the frequency of 50 MHz, when the two random variables are θ and ψ.

SROM method gives a more accurate CDF compared to that of SC. However, at the sample size of 29, the CDF given by SC becomes very close to the reference CDF, whereas the SROM-based CDF is still noticeably different (although significantly improved compared to the CDF at 13 samples). This noticeable discrepancy from the staircase-shaped CDF is due to the discontinuity nature of the CDF approximation mechanism in (8). To improve the resolution of the SROM-based CDF, one needs to increase the sample size. Seeing the 65 sample case in Fig. 5 for example, the difference between the SROM-based and reference CDFs becomes almost indistinguishable. Finally, at the sample size of 145, both methods give the error-free CDF of I_{R3}. In Fig. 5, no method shows overwhelming accuracy over the counterpart to predict the CDF of the induced current I_{R3} in the case of random incidence angles θ and ψ.

As shown in Fig. 6, the performances of the SROM and SC methods to estimate the mean value μ and standard deviation σ of the induced current I_{R3} are compared at the sample sizes of 5, 13, 29, 65, 145, 321, 705, 1537, and 3329, corresponding to $k = 1, 2, \ldots$, and 9, respectively. It is clear that in this case the SROM method is more efficient than the SC method to converge with sufficient accuracy. Specifically, the SROM method only needs 13 samples to produce accurate μ (I_{R3}) and σ (I_{R3}) (both within the error of 2% with respect to the MC result using 200000 simulations). In contrast, at least 145 collocation points are required for the SC-based μ (I_{R3}) and σ (I_{R3}) to simultaneously converge to the SROM accuracy level at the sample size of 13. The reason is that the approximated response of I_{R3} by the SC method only becomes sufficiently detailed when using 145 collocation points or more. This can be clearly demonstrated using Fig. 7. Specifically, Fig. 7(a) shows 145 collocation points in the uncertain input region, and Fig. 7(b) shows a good match between the approximated and theoretical responses of I_{R3}. Therefore, to obtain accurate μ (I_{R3}) and σ (I_{R3}) in the presence of uncertain θ and ψ, the number of repeated deterministic runs can be reduced by a factor of $145/13 \approx 11$ by replacing the SC method with the SROM method. Finally, the MC method needs around 9000 simulations to converge to the same accuracy level. Hence, the MC process can be expedited by $9000/13 \approx 692$ times using the SROM method.

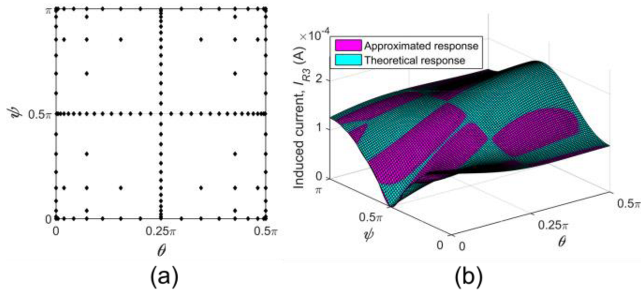

FIGURE 7. (a) 145 collocation points obtained using sparse grids based on the extrema of Chebyshev polynomials, with $D = 2$ and $k = 5$. (b) Comparison of the theoretical response and the SC approximated response using 145 collocation points.

Instead of aforementioned discussion at the single frequency of 50 MHz, the comparison between the SROM and SC performances is widened to the frequency range: [10 MHz, 100 MHz] in Fig. 8. It is clear that at the sample size of 13, the SROM-based μ (I_{R3}) and σ (I_{R3}) are more accurate than the SC results, especially at the resonance frequency around 80 MHz. It is interesting to see that the errors are increasing when dealing with resonance frequency. This shows that the quality of the approaches could be subject to the complexity of the deterministic mapping. More specifically, the resonating nature of the problem makes the induced current more sensitive to random incidence angles, and consequently degrades the result accuracy.

As shown above, accurate mean value μ and standard deviation σ of the induced current I_{R3} can be obtained at each frequency using the SROM method with 13 samples. For practical purposes, the interval $[\mu-3\sigma, \mu+3\sigma]$ can be

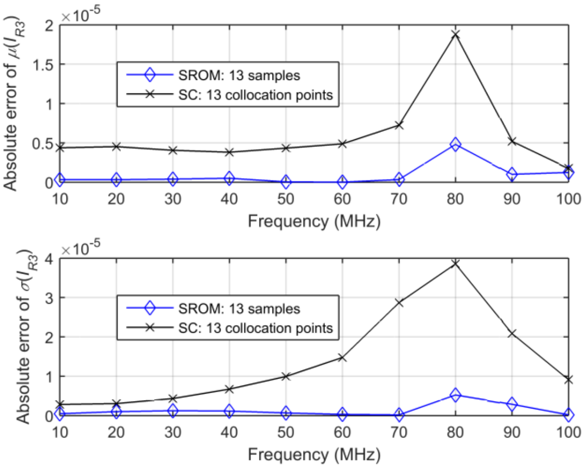

FIGURE 8. Comparison of the SROM and SC performances to estimate the mean value μ (I_{R3}) and standard deviation σ (I_{R3}) in the frequency range: [10 MHz, 100 MHz].

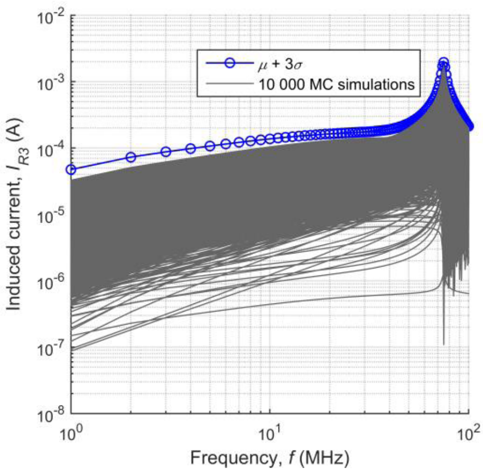

FIGURE 9. Upper bound of the induced current I_{R3} obtained using the SROM method with only 13 samples, in the presence of the two random variables: θ and ψ.

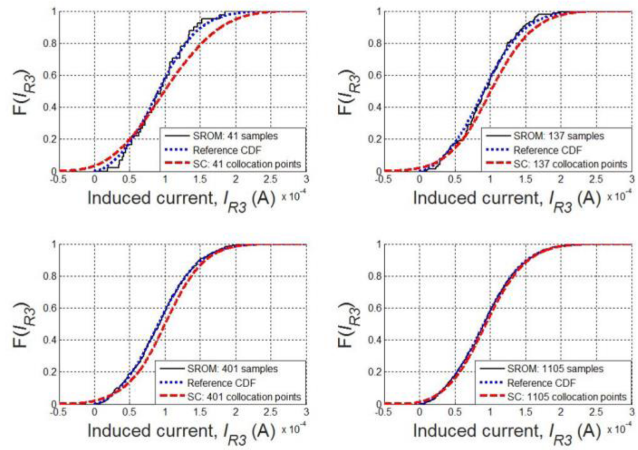

FIGURE 10. Comparison of the reference CDF of I_{R3}, the CDFs approximated by the SROM-based output $\tilde{I}_{R3}$ with the sample sizes of 41, 137, 401, and 1105, and the CDFs approximated by the SC method with 41, 137, 401, and 1105 collocation points (corresponding to $k = 2, 3, 4$, and 5, respectively).

used as a heuristic and general choice to define approximate upper and lower bounds. On this basis, the variability of I_{R3} can be bounded. To ensure it is worth assuming $\mu+3\sigma$ as the maximum, one may need to validate with high quantile assessment (such as 0.95, 0.99, 0.995 quantile), which is beyond the scope of this paper. Please note that Fig. 9 only presents the upper boundary in the frequency range: [1 MHz, 100 MHz]. This is because: 1) the upper bound is of more interest for field-to-wire coupling problems, and 2) the lower bound based on $\mu-3\sigma$ could give minus (i.e., not physically sound) induced currents at some frequencies, and, therefore, is omitted in Fig. 9. As shown in Fig. 9, it is remarkable that the accurate upper boundary obtained using only 13 SROM samples (i.e., 13 simulations) can hold underneath almost 10000 random simulation results. Comparing 13 simulations by SROM to 10000 simulations by MC, it is obvious to see the sizable acceleration given by the SROM method.

B. RANDOM θ, ψ, η, AND E_0

In this section, the incident plane-wave field is assumed to be fully stochastically characterized by all four random variables: the incidence angles θ and ψ, field strength E_0, and polarization angle η. To further complicate the investigated problem, random variables are assumed to follow different probability distribution types. Specifically, the random variables θ, ψ, and η are uniformly distributed in the ranges $[0, \pi/2]$, $[0, \pi]$, and $[0, 2\pi]$, respectively. These variation ranges of the angles cover all possible physical values of the plane wave in the upper half-space without redundancy. Also, E_0 is regarded as a Gaussian random variable with the mean value $E(E_0) = 1$ V/m and standard deviation $\sigma(E_0) = 0.2$ V/m.

In this case, the SROM-based input $\tilde{X}$ needs to be constructed for the 4-D random variable $X = [\theta, \psi, E_0, \eta]$. For the SC method, at the random dimension $D = 4$, the number of collocation points based on sparse grid sampling is 9, 41, 137, 401, 1105, 2929, and 7537, corresponding to $k = 1, 2, 3, 4, 5, 6$, and 7, respectively. It is worth noting the efficiency of sparse grid sampling over tensor product sampling in this case. Specifically, the top three minimum numbers of collocation points based on tensor product sampling are $2^4 = 16$, $3^4 = 81$, and $4^4 = 256$, and can be reduced to 9, 41, and 137 using sparse grid sampling. Again, the sample sizes for the SROM and SC methods are the same in each comparison. The implementation of the SROM and SC methods follows the same process demonstrated in Section IV-A, and, therefore, is not detailed herein.

Fig. 10 shows the CDFs of the induced current I_{R3} given by the SROM and SC methods using the sample sizes of 41, 137, 401, and 1105. Clearly, the CDF given by each method becomes more accurate by increasing the sample size. But the SROM-based CDF is generally more accurate than the SC-based CDF. At the sample sizes of 137 and 401, the

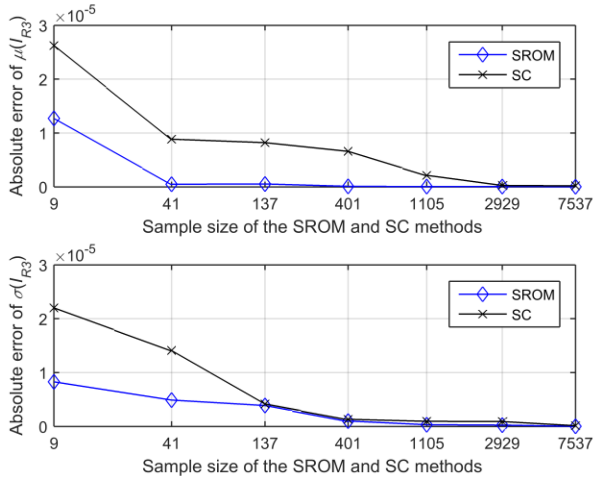

FIGURE 11. Convergence rates of the SROM and SC methods at the frequency of 50 MHz, when the four random variables are θ , ψ, E_0, and η.

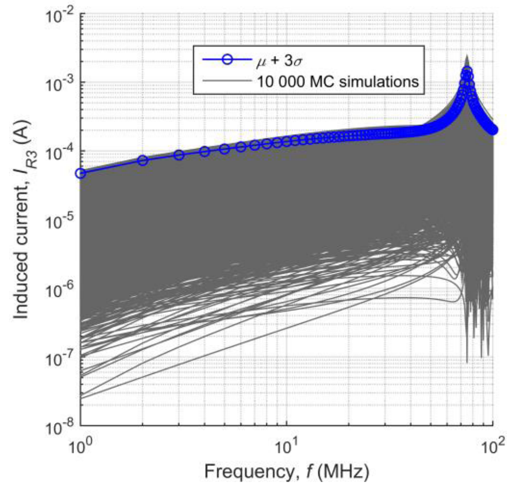

FIGURE 12. Upper bound of the induced current I_{R3} obtained using the SROM method with 41 samples, in the presence of the four random variables: θ , ψ, E_0, and η.

CDFs given by SROM are already in good agreement with the reference CDF, whereas the CDFs given by SC exhibit obvious discrepancy. The SC method can only produce accurate CDFs by using 1105 collocation points. This is because at least 1105 collocation points are needed to give sufficient resolution to the SC approximated response of I_{R3}. Please note that in this example, the SC method could generate minus (i.e., non-physical) induced currents at the sample size of 41, due to the insufficient resolution of the approximated response. This behavior could contaminate the statistical information of the induced current. To resolve this problem, one should increase the number of SC collocation points, thus to increase the resolution of the approximated response. Please see the reduced probability of the non-physical current in the 137 sample case in Fig. 10 for example.

In Fig. 11, the convergence rates of the SROM and SC methods are compared at the sample sizes of 9, 41, 137, 401, 1105, 2929, and 7537. It is clear that in this case, the SROM method is more efficient than the SC method to obtain the converged mean value $\mu(I_{R3})$ and standard deviation $\sigma(I_{R3})$. Specifically, the sample size of 401 is sufficient for the SROM method to converge to accurate $\mu(I_{R3})$ and $\sigma(I_{R3})$, both within the error of 2%. In contrast, the SC method needs at least a sample size of 1105 to converge to around the same accuracy level. This is in line with the accurate SC-based CDF given by 1105 collocation points in Fig. 10. By switching from the SC method to the SROM method, the number of deterministic runs needed for accurate results can be reduced by a factor of $1105/401 \approx 2.8$. Meanwhile, the MC method needs around 23000 simulations to converge to the SROM accuracy level at the sample size of 401. Therefore, the MC analysis can be expedited by $23000/401 \approx 57$ times using the SROM method. Please note that each method (SROM, SC, and MC) needs a larger sample size to converge in this case than in Section IV-A, due to the increment of the random dimension. Please note that the convergence rate of SC in Fig. 11 does not exhibit the exponential feature claimed in [28]. This is because the efficacy of SC can be influenced by the complexity of the deterministic mapping between the input and the output. It is worth noting that the SROM-based μ (I_{R3}) and σ (I_{R3}) at the sample size of 41 are already accurate to some extent, specifically with the errors of 1% and 7%, respectively.

On this basis, Fig. 12 shows the heuristic upper bound of the induced current I_{R3} obtained by the SROM method with the sample size of 41. It is clear that almost 10000 MC simulations (except for very few extreme occurrences) are held underneath this upper bound. Therefore, the efficiency of obtaining the upper bound is remarkable using the SROM method. It is interesting to see that the spread of I_{R3} in Fig. 12 for the 4-D case is wider than that in Fig. 9 for the 2-D case. This is because there are many more possible occurrences in the 4-D case.

V. DISCUSSION

This section presents in-depth discussions on the performances of SROM and SC in the 2-D and 4-D examples. It is clear that both the SROM and SC methods are much more efficient than the MC method. Also, the comparison between SROM and SC shows that the SROM method has a faster convergence rate to produce accurate statistics of the induced current I_{R3}. On the other hand, as shown in the 4-D case, the SC method may generate non-physical induced currents, making the SC result considerably deviate from the reference. However, please note that the presented SC result is given by standard implementation based on sparse grid sampling, but state-of-the-art SC variations (such as the adaptive sparse grid collocation method [22]) are possible, and may produce better performance. The non-intrusive PCE method [28] may also outperform the SROM method in terms of accuracy and computational cost. However, the comparison with every competing technique would be too exhaustive. There is no intention of contriving the examples and results in this paper to make SROM appear as superior. The demonstrated goodness of the SROM method over the SC method only holds true in the scope of this paper, and may become overstated in other cases.

It should be pointed out that the distribution of the output is described via CDF using the SROM method. In fact, the probability density function may be better to show the shape of the distribution tails and estimate the spreading of the system response. But due to the nature of the SROM-based output (i.e., consisting of a set of discrete sample-probability pairs), it may be unfeasible to produce a continuous PDF directly by SROM. Please note that the performance of MC regarding mean, standard deviation, and CDF prediction is neglected in the examples. This is because at such sample sizes, performing a MC analysis with the same number of samples for different values of the random variables considered gives very different results.

TABLE 2. Computation time required by SROM, SC, and MC.

Example		X=[θ, ψ]	X=[θ, ψ, E_0, η]
SROM	Time (s)	0.4	5.9
	Speed-up	367×	63×
SC	Time (s)	8.3	22.1
	Speed-up	18×	17×
MC	Time (s)	146.7	372.5
	Speed-up	-	-

Although both the SROM and SC methods need to repeatedly call the deterministic solver, the overall complexity of each method is different. This is because the core of the SROM implementation is to construct an accurate SROM-based input. Then, the statistics of the output can be straightforwardly obtained using (8)-(10). In contrast, the SC method needs to first select collocation points based on sparse grids, and then derive the approximated response of the output before quantifying the output uncertainty. Table 2 shows the computation time required by each method to converge within the error of 2%, and the speed-up factor compared with MC, based on a CPU of 3.4 GHz and RAM of 8 GB. The MC simulation time in Table 2 refers to 9000 simulations for the example $\boldsymbol{X} = [\theta, \psi]$ and 23000 simulations for $\boldsymbol{X} = [\theta, \psi, E_0, \eta]$. It is clear that the SROM implementation is faster than SC, and much faster compared to the MC method.

Some questions about the SROM method are still waiting to be solved. For example, there is still no clear guideline on how to choose the optimal sample size m of $\tilde{\boldsymbol{X}}$, given probability distribution types and the number of dimensions. Also, the performances of the SROM and SC methods in Section IV are based on *a-posteriori* evaluation. This means that the accuracy of each method can only be revealed after comparing the result to the reference. In fact, an *a-priori* evaluation approach would be more desirable. However, this task is extremely difficult. The reason is that the accuracy of the SROM solution is not solely dependent on the SROM approximation of the real input, but also affected by the deterministic mapping (i.e., the problem under investigation). As a result, the *a-priori* accuracy evaluation should be tailored to each specific EMC problem. At the current stage, proposing a general guideline still remains as a bottleneck. On the other hand, it will be worth investigating how the SROM method scales with the number of random variables, given a practical computational resource. However, it may be difficult to yield a general conclusion. This is because the sensitivity of the output to random variables is different in each problem, which could affect the efficacy of the SROM method.

It is worth noting that the cable in this paper is assumed to be a uniform transmission line with lossless and bare wires. It would certainly be more practical and convincing to consider the cable with some real features. However, this assumption is acceptable in the scope of this paper. This is because all the uncertainty sources are assumed to be embedded in the incident plane-wave field. This random field is the nucleus component of the statistical analysis. The cable itself is only used as a victim for the current to be induced to.

VI. CONCLUSION

In this paper, a nonintrusive statistical approach referred to as the SROM method has been applied to efficiently estimate the statistics of the induced current in transmission lines excited by a random incident plane-wave field. The robustness of the SROM method has been validated by assuming the incident wave to be fully statistically characterized. With the SROM method, the accurate statistical information of the induced current (such as the CDF, mean value, standard deviation, and the upper bound) has been obtained with great efficiency.

The performance of the SROM method has been thoroughly compared with other nonintrusive statistical approaches (SC and MC) for the prediction of the field-to-wire coupling phenomenon. It has been found that the SROM method is more efficient than the SC method in terms of reducing the number of simulations, and much more efficient than the MC method in the examples considered. The advantages and limitations of the SROM method have been thoroughly discussed, such as the implementation simplicity and the difficulty of developing the *a-prior* error evaluation mechanism.

Having demonstrated the impressive accuracy and efficiency of the SROM method in a typical field-to-wire coupling problem, the idea of the SROM method can be suggested to expedite statistical irradiation analysis in complex platforms (such as the cable in aircrafts).

REFERENCES

[1] C. Taylor and C. Harrison, Jr., "The response of a terminated two-wire transmission line excited by a nonuniform electromagnetic field," *IEEE Trans. Antennas Propag.*, vol. 13, no. 6, pp. 987–989, Nov. 1965.

[2] C. R. Paul, "Frequency response of multiconductor transmission lines illuminated by an electromagnetic field," *IEEE Trans. Electromagn. Compat.*, vol. EMC-18, no. 4, pp. 183–190, Nov. 1976.

[3] C. R. Paul, *Analysis of Multiconductor Transmission Lines*, 2nd ed. New York, NY, USA: Wiley, 2008.

[4] R. B. Armenta and C. D. Sarris, "Efficient evaluation of the terminal response of a twisted-wire pair excited by a plane-wave electromagnetic field," *IEEE Trans. Electromagn. Compat.*, vol. 49, no. 3, pp. 698–707, Aug. 2007.

[5] S. A. Pignari and G. Spadacini, "Plane-wave coupling to a twisted-wire pair above ground," *IEEE Trans. Electromagn. Compat.*, vol. 53, no. 2, pp. 508–523, May 2011.

[6] G. Spadacini, F. Grassi, F. Marliani, and S. A. Pignari, "Transmission-line model for field-to-wire coupling in bundles of twisted-wire pairs above ground," *IEEE Trans. Electromagn. Compat.*, vol. 56, no. 6, pp. 1682–1690, Dec. 2014.

[7] M. Omid, Y. Kami, and M. Hayakawa, "Field coupling to nonuniform and uniform transmission lines," *IEEE Trans. Electromagn. Compat.*, vol. 39, no. 3, pp. 201–211, Aug. 1997.

[8] G. Spadacini and S. A. Pignari, "Numerical assessment of radiated susceptibility of twisted-wire pairs with random nonuniform twisting," *IEEE Trans. Electromagn. Compat.*, vol. 55, no. 5, pp. 956–964, Oct. 2013.

[9] G. Antonini, S. Cristina, and A. Orlandi, "PEEC modeling of lightning protection systems and coupling to coaxial cables," *IEEE Trans. Electromagn. Compat.*, vol. 40, no. 4, pp. 481–491, Nov. 1998.

[10] F. Rachidi, "A review of field-to-transmission line coupling models with special emphasis to lightning-induced voltages on overhead lines," *IEEE Trans. Electromagn. Compat.*, vol. 54, no. 4, pp. 898–911, Aug. 2012.

[11] A. Papoulis, *Probability, Random Variables and Stochastic Processes*, 3rd ed. New York, NY, USA: McGraw-Hill, 1991.

[12] D. Bellan and S. Pignari, "A probabilistic model for the response of an electrically short two-conductor transmission line driven by a random plane wave field," *IEEE Trans. Electromagn. Compat.*, vol. 43, no. 2, pp. 130–139, May 2001.

[13] D. Bellan and S. Pignari, "Probability density function of load voltages in randomly excited multiconductor transmission line," *Electron. Lett.*, vol. 36, no. 19, pp. 1606–1607, Sep. 2000.

[14] M. Larbi, P. Besnier, B. Pecqueux, and F. Puybaret, "Plane wave coupling to an aerial electrical cable. Assessment of extreme interference levels with the controlled stratification method," in *Proc. EMC EUROPE*, Wroclaw, Poland, Sep. 2016, pp. 112–117.

[15] C. P. Robert and G. Casella, *Introducing Monte Carlo Methods With R*. New York, NY, USA: Springer, 2009.

[16] D. Xiu and G. E. Karniadakis, "The Wiener–Askey polynomial chaos for stochastic differential equations," *SIAM J. Sci. Comput.*, vol. 24, no. 2, pp. 619–644, Jul. 2002.

[17] D. Xiu, "Efficient collocational approach for parametric uncertainty analysis," *Commun. Comput. Phys.*, vol. 2, no. 2, pp. 293–309, Apr. 2007.

[18] M. Grigoriu, "Reduced order models for random functions. Application to stochastic problems," *Appl. Math. Model.*, vol. 33, no. 1, pp. 161–175, Jan. 2009.

[19] S. Pignari and D. Bellan, "Statistical characterization of multiconductor transmission lines illuminated by a random plane-wave field," in *Proc. IEEE Int. Sym. EMC*, Washington, DC, USA, Aug. 2000, pp. 605–609.

[20] G. Spadacini, F. Grassi, and S. Pignari, "Statistical properties of low frequency voltages induced by a plane-wave field across the terminal loads of a random wire-bundle," in *Proc. IEEE Int. Sym. EMC*, Dresden, Germany, Aug. 2015, pp. 824–829.

[21] P. Manfredi and F. G. Canavero, "Polynomial chaos for random field coupling to transmission lines," *IEEE Trans. Electromagn. Compat.*, vol. 54, no. 3, pp. 677–680, Jun. 2012.

[22] B. Ganapathysubramanian and N. Zabaras, "Sparse grid collocation schemes for stochastic natural convection problems," *J. Comput. Phys.*, vol. 225, no. 1, pp. 652–685, Jul. 2007.

[23] Z. Fei, Y. Huang, J. Zhou, and Q. Xu, "Uncertainty quantification of crosstalk using stochastic reduced order models," *IEEE Trans. Electromagn. Compat.*, vol. 59, no. 1, pp. 228–239, Feb. 2017.

[24] S. Sarkar, J. E. Warner, W. Aquino, and M. Grigoriu, "Stochastic reduced order models for uncertainty quantification of intergranular corrosion rates," *Corrosion Sci.*, vol. 80, pp. 257–268, Mar. 2014.

[25] Q. Du, V. Faber, and M. Gunzburger, "Centroidal Voronoi tessellations: Applications and algorithms," *SIAM Rev.*, vol. 41, no. 4, pp. 637–676, Oct. 1999.

[26] S. Pignari and F. G. Canavero, "Theoretical assessment of bulk current injection versus radiation," *IEEE Trans. Electromagn. Compat.*, vol. 38, no. 3, pp. 469–477, Aug. 1996.

[27] A. Klimke. (May 25, 2008). *Sparse Grid Interpolation Toolbox*. [Online]. Available: http://www.ians.unistuttgart.de/spinterp/index.html

[28] M. S. Eldred, "Recent advance in non-intrusive polynomial chaos and stochastic collocation methods for uncertainty analysis and design," in *Proc. 50th AIAA/ASME/ASCE/AHS/ASC Struct., Struct. Dyn., Mater. Conf.*, Palm Springs, CA, USA, May 2009, pp. 1–37.

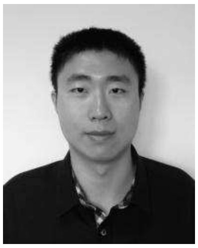

ZHOUXIANG FEI was born in Xi'an, China, in 1990. He received the B.Eng. degree in electronics and information engineering from Northwestern Polytechnical University, Xi'an, China, in 2012 and the M.Sc. degree (Hons.) in wireless communications from the University of Southampton, Southampton, U.K., in 2013. He is currently pursuing the Ph.D. degree with the University of Liverpool, Liverpool, U.K. His current research interests include numerical and experimental studies of crosstalk in complex cable bundles, with a particular emphasis on considering parameter variability using efficient statistical approaches. He was a recipient of the student scholarship from the IEEE EMC Society to attend the 2016 IEEE International Symposium on EMC, Ottawa, Canada, 2016. He was also selected as the Best EMC Paper Finalist for the 2016 IEEE International Symposium on EMC.

YI HUANG (S'91–M'96–SM'06) received the B.Sc. degree in physics from Wuhan University, China, in 1984, M.Sc. degree in microwave engineering, Nanjing Research Institute of Electronics Technology, Nanjing, China, in 1987, and D.Phil. degree in communications from the University of Oxford, U.K. in 1994. He has been conducting research in the areas of wireless communications, applied electromagnetics, radar, and antennas since 1987. His experience includes 3 years spent with NRIET as a Radar Engineer and various periods with the Universities of Birmingham, Oxford, and Essex, U.K. as a Member of Research Staff. He was a Research Fellow with British Telecom Labs in 1994, and then was with the Department of Electrical Engineering and Electronics, the University of Liverpool, U.K. as a Faculty in 1995, where he is currently a Full Professor in wireless engineering, the Head of High Frequency Engineering Group and Deputy Head of Department. He has authored over 300 refereed papers in leading international journals and conference proceedings, and authored Antennas: from Theory to Practice (John Wiley, 2008) and Reverberation Chambers: Theory and Applications to EMC and Antenna Measurements (John Wiley, 2016). He has received many research grants from research councils, government agencies, charity, EU, and industry, acted as a Consultant to various companies, and served on a number of the National and International Technical Committees and been an Editor, Associate Editor or Guest Editor of four of international journals. He has been a keynote/invited speaker and organizer of many conferences and workshops (e.g. WiCom 2006, 2010, IEEE iWAT2010, and LAPC2012). He is currently the Editor-in-Chief of Wireless Engineering and Technology, Associate Editor of the IEEE Antennas and Wireless Propagation Letters, U.K. and Ireland Representative to European Association of Antenna and Propagation, a Fellow of IET, and Senior Fellow of HEA.

JIAFENG ZHOU received the B.Sc. degree in radio physics from Nanjing University, Nanjing, China, in 1997, the Ph.D. degree from the University of Birmingham, Birmingham, U.K., in 2004. His doctoral research concerned high-temperature superconductor microwave filters. From 1997, for two and a half years he was with the National Meteorological Satellite Center of China, Beijing, China, where he was involved with the development of communication systems for Chinese geostationary meteorological satellites. From 2004 to 2006, he was a Research Fellow with the University of Birmingham, where his research concerned phased arrays for reflector observing systems. He was with the Department of Electronic and Electrical Engineering, University of Bristol, Bristol, U.K. until 2013. His research in Bristol was on the development of highly efficient and linear amplifiers. He is currently with the Department of Electrical Engineering and Electronics, University of Liverpool, Liverpool, U.K. His current research interests include microwave power amplifiers, filters, electromagnetic energy harvesting, and wireless power transfer.

CHAOYUN SONG (S'16) was born in Gansu, China, in 1990. He received the B.Eng. degree (Hons) in telecommunication engineering from Xi'an Jiao Tong Liverpool University, Suzhou, China, in 2012, the M.Sc. degree (Hons.) in microelectronics and telecommunication from the University of Liverpool, Liverpool, U.K. in 2013. He is currently pursuing the Ph.D. degree in wireless communications and RF engineering with the University of Liverpool, U.K. He has been a regular reviewer of 2 IEEE Transactions. His current research interests include rectifying-antenna, circular polarization antenna, power management circuit, wireless power transfer and energy harvesting, and wearable antennas.